

# Probabilistic lithofacies classification with machine learning application for improved confidence in subsurface modelling

Tanmay Singh<sup>1</sup>, Pradyut Laha<sup>1</sup>, Nabin Mandal<sup>1</sup> and Partha Pratim Mandal<sup>1</sup>

#### **ABSTRACT**

Classifying lithofacies is essential for understanding geological variability in hydrocarbon reservoirs. Machine learning (ML) tools are increasingly used to classify lithofacies for reservoir characterization. In this study, we implemented three ML classification algorithms: Multilayer Perceptron (MLP), Random Forest (RF), and CNN-Shift Padding model to output each individual probabilistic facies class in a range of 0 to 1 using an open-source dataset from the Hugoton and Panoma gas fields, Southwest Kansas, USA. The dataset consists of 4,149 samples from 10 wells with facies identified from core description where each well is characterized by five wireline logs and two derived geological properties. Additional input features and missing data was generated as part of data quality control and data conditioning. To better reflect geological continuity, predictions were evaluated using both exact facies labels and geologically reasonable adjacent facies labels. While RF and MLP yielded comparable predictive metrices, the performance of MLP model was found optimal, achieving higher blind well prediction accuracies when adjacent facies are considered. Incorporation of probability-based facies prediction helped to quantify model confidence and to identify ambiguous zones, particularly within transitional intervals or thin beds. Results show that MLP model reliably detects thin layers of Phylloid-Algal Bafflestone (BS), a critical gas-bearing facies with higher porosity and permeability, even with limited training samples. Overall, the study demonstrates that integrating additional input features, adjacent facies adjustment, and probability thresholding provides a robust framework for lithofacies prediction. The approach improves accuracy beyond previously reported benchmarks and enhances interpretability by quantifying prediction confidence, thereby supporting reliable geological modelling and reservoir characterization in wells lacking core samples.

#### **KEYWORDS**

Lithofacies, probability, machine learning, classification, multilayer perceptron

# **INTRODUCTION**

Machine learning (ML) has demonstrated significant success in providing data-driven solutions in diverse scientific disciplines and has emerged as a powerful tool

in geoscience to improve subsurface characterization and decision-making. ML comprises a group of data algorithms that include classification, analysis regression, and clustering methods (Hall, 2016). In lithofacies analysis, conventional manual and simplistic statistical approaches are often time-consuming and labour-intensive, limited in scalability, and unable to capture the complexity of subsurface heterogeneity. With the shift towards contemporary non-parametric methods such as Artificial Neural Network (ANN), fuzzy logic, principal component analysis (PCA), and other advanced classification algorithms (Dubois et al., 2007; Hall, 2016), supervised machine learning approaches enable the extraction of subtle patterns from wireline logs and facilitates lithofacies prediction in wells lacking core data. Core samples remain essential for accurately labelling rock types, as they provide direct petrophysical sedimentological information. Since core acquisition is costly and limited to a few wells within reservoir, supervised models trained on cored intervals are commonly applied to uncored wells from the available wireline logs (Dubois et al., 2007). However, deterministic facies classifications may not adequately represent uncertainty, which is a critical aspect for reliable reservoir modelling and simulation. In this regard, probabilistic machine learning offers a more robust framework by not only predicting lithofacies but also quantifying confidence levels, ultimately improving subsurface modelling and reducing decision-making risks.

The present study comprised five wireline log curves over 10 wells that included gamma ray (GR), logarithmic value of resistivity (ILD\_log10), photo-electric factor (PE), neutron-density porosity difference (DeltaPHI), and average neutron-density porosity (PHIND). PE curves are missing in a few wells, which is a vital input feature for the rock-type classification problem. The dataset also contains two geological constraining variables, *viz.* non-marine and marine identifier (NM and M), and relative position defined as RELPOS. We implemented non-

<sup>1</sup>Subsurface Resource Characterization Group, Department of Applied Geophysics, IIT(ISM), Dhanbad

Emails: Tanmay: 24dr0207@iitism.ac.in; Pradyut: 23mc0056@iitism.ac.in; Nabin: 23mc0051@iitism.ac.in; partham@iitism.ac.in

linear machine learning regression techniques to produce synthetic PE logs where input features are basic wireline logs. We considered the whole dataset including additional PE synthetic logs for rock-type prediction. The studied sedimentary rock comprised of nine lithofacies classes as reported by (Dubois et al., 2007), which were labelled through detailed and rigorous petrophysical evaluation and core analysis. We termed them in short nomenclature throughout this paper, which are listed in Table 1.

**Table-1**: Facies nomenclature with adjacent facies. (Dubois et al., 2007)

Facies	Description	Acronyms	Adjacent facies		
1	Non-marine sandstone	SS	2		
2	Non-marine coarse siltstone	CSiS	1,3		
3	Non-marine fine siltstone	FSiS	2		
4	Marine siltstone and shale	SiSh	5		
5	Mudstone	MS	4,6		
6	Wackstone	WS	5,7,8		
7	Dolomite	D	6,8		
8	Packstone-grainstone	PS	6,7,9		
9	Phylloid-algal bafflestone	BS	7,8		

According to Dunham's carbonate rock texture classification (Dunham, 1962), MS, WS, and PS are combination of mud and grain supported carbonate rocks, which makes their distinction challenging due to subjective gradational boundaries, grain-size estimation, and the difficulty of recognizing baffling structures. Figure 1 shows the facies distribution across different wells in the dataset. Each bar represents the total count of facies within a well, with colours corresponding to the nine facies classes. This plot highlights both the variability in facies occurrence and the imbalance in facies representation across wells. Previously published Hall's work predicted 43% accuracy on a blind well with the application of the support vector machine classifier algorithm (Hall, 2016). The present approach considered three non-parametric supervised ML classification algorithms: Multi-layer perceptron (MLP), Random Forest (RF), and Convolution Neural Network with Shift padding (CNN-shift). Then we compared to choose the best algorithm by observing classification metrics on cross-validation samples.

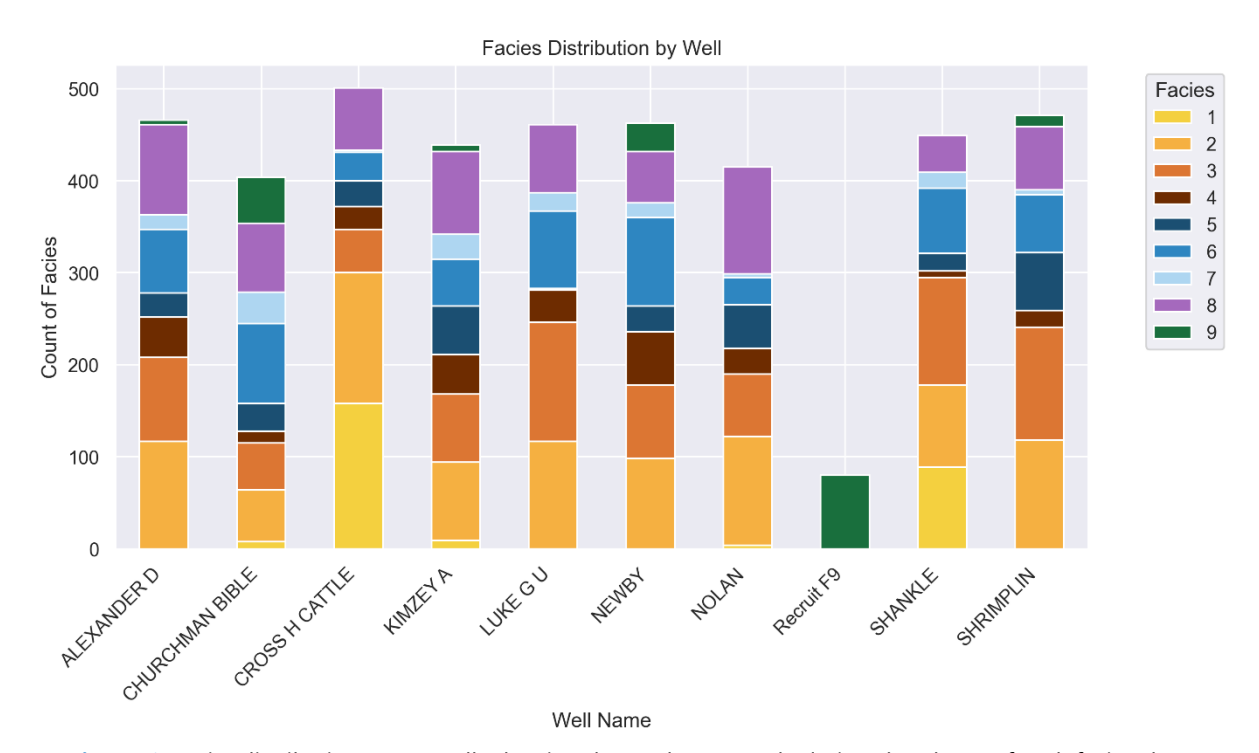


Figure 1: Facies distribution across wells showing the total count and relative abundance of each facies class.

Finally, a comparative analysis has been conducted between the probability scores of above 0.50 and 0.90 to report the advantages and limitations of traditional machine learning approaches in achieving accurate facies classification.

This study signifies the ability of probabilistic outcome of machine learning algorithms to capture lithofacies

transitions and quantify uncertainty, while comparing algorithmic performance against previously reported approaches (Hall, 2016). This work further explores the implications of probability-driven facies mapping for subsurface modelling, particularly in identifying reservoir-prone facies.

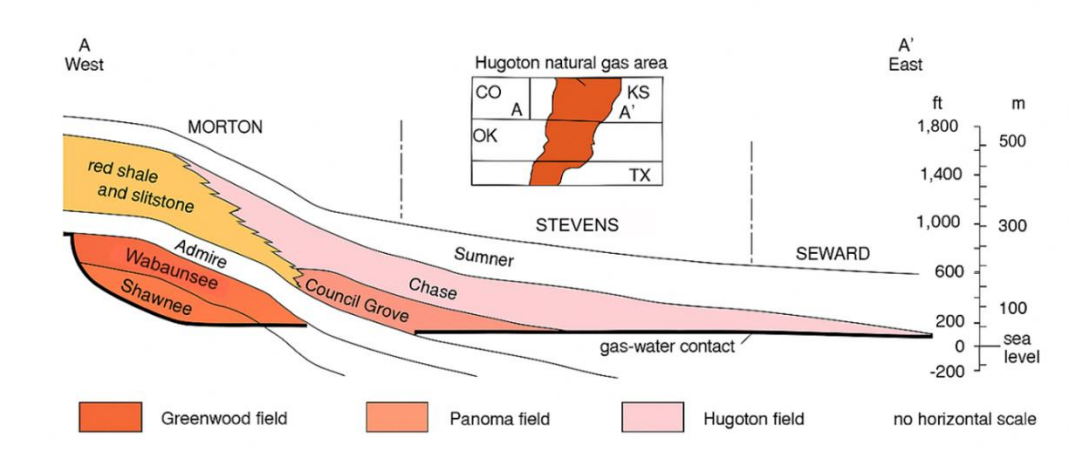


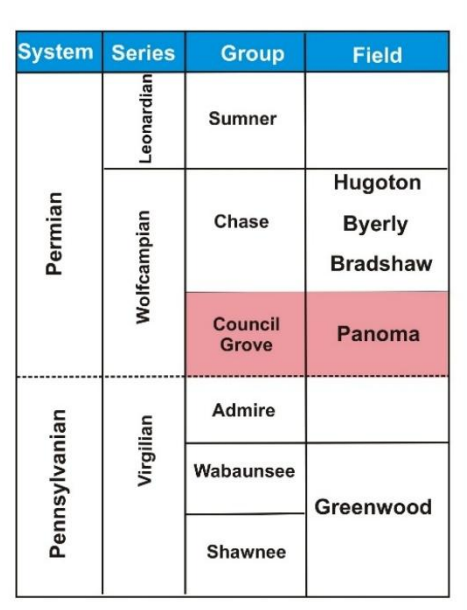
Figure 2: Schematic vertical section (West-East) of the Hugoton and Panoma gas field. Modified from Kansas Geological Survey (Carr and Sawin, 1997)

# **STUDY AREA**

The Hugoton Gas Field is one of the largest natural gas accumulations in North America, located primarily in western Kansas as a northern shelf extending into larger and deeper subsurface into Oklahoma and Texas, known as the Anadarko basin (Mazzullo, 1998). Geologically, comprises Permian-age the region carbonates (limestones and dolomites) and siliciclastic deposits resulting from subsequent marine transgression and regressions on a gently sloping shelf (Dubois et al., 2006). The field's primary hydrocarbon trap results from lateral facies changes. Moving westward and up-dip, the porous marine limestones and dolomites of the Chase and Council Grove Groups transition into tight red shales, with the Council Grove group restricted to the Panoma field, which lies beneath and is geologically overlapped by the Hugoton Field (Figure 2) (Hemsell, 1939). This facies pinch-out forms a regional stratigraphic seal that confines gas within the permeable carbonates. The internal heterogeneity of the reservoir arises from the complex interlayering of grainsupported carbonates primarily windblown silts, very

fine sands and clay rich silts with paleosols. The main pay zones are continuous across broad areas, but the vertical connectivity of these reservoirs may be restricted by laterally persistent nonmarine siltstones and shales (Figure 3) (Olson et al., 1997). The Panoma Field is strongly associated with the Hugoton and is characterized by similar stratigraphic units but exhibits unique facies and depositional cycles. There are strong lateral facies variations, from thick nonmarine shale and silt (northwest) to marine carbonates (southeast). These facies changes create stratigraphic traps by laterally grading porous carbonates into tighter, nonmarine packages, directly impacting reservoir quality and geometry (Halotel et al., 2020).

Depositional cyclicity in both the Hugoton and Panoma Fields plays a defining role in their reservoir architecture, with each field exhibiting vertically stacked sequences of alternating marine and nonmarine intervals that were deposited in response to rapid, glacially driven sea-level fluctuations during the Permian period. These repeated fourth-order transgression-regression cycles generate characteristic shoaling-upward successions, where



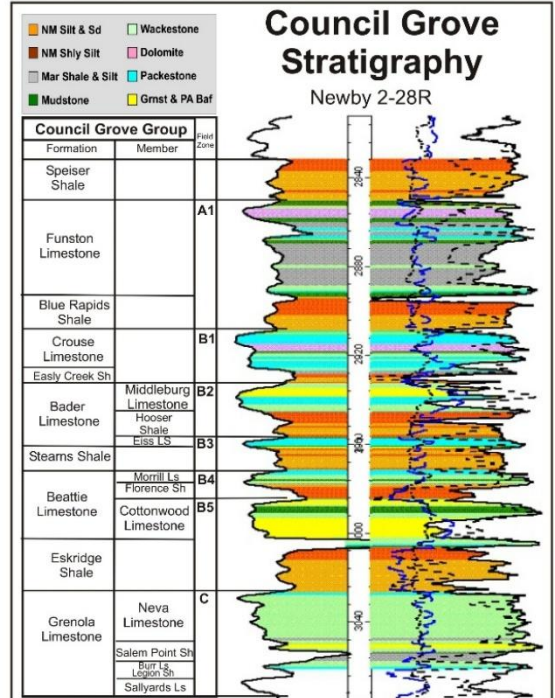
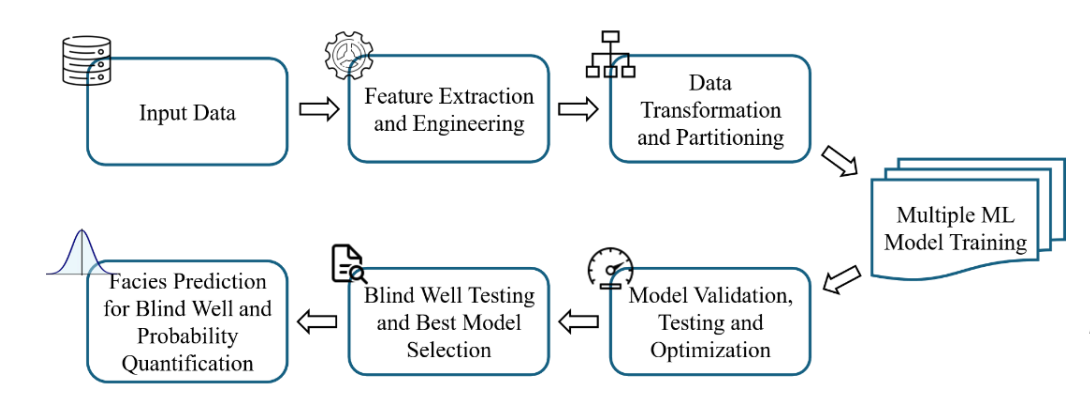


Figure 3: Stratigraphy of the Council Grove demonstrating the geological complexity with the marine and non-marine sequences bounded by unconformities on exposed carbonate surfaces. (Kansas Geological Survey, 2003)



**Figure 4**: Machine learning classification pipeline applied in the current study for facies prediction and probability quantification.

porous marine carbonates are overlain by tighter nonmarine shale and siltstone beds (Figure 3). This vertical pattern produces a complex stratigraphy, filling the reservoirs with significant heterogeneity both vertically and laterally, and results in intervals of widely varying reservoir quality and connectivity.

Accurate identification and mapping of these cyclic successions, such as their location, thickness, and extent, are fundamental for effective reservoir simulation, modelling, and optimal field development, as they

directly influence pay zone prediction, hydrocarbon recovery, and well performance in these giant, mature gas fields.

# **METHODOLOGY**

Any ML problem can be broadly structured into five key stages, as illustrated by the workflow diagram in Figure 4. Critical stages include the preparation of input datasets, assessment of statistical significance, and visualization of the input-output mapping function, which is essential for the success of an ML project.

Quality control of well log data was performed to ensure the reliability and consistency of the dataset prior to analysis. As can be observed from Figure 5 (half-violin plots), the data distribution is illustrated by combining kernel density estimation (KDE) with conventional box plot statistics. The half-violin shape reflects the probability density of the data across the measured range, providing insight into distribution asymmetry and spread. Within the half-violin, the embedded box plot marks the interquartile range (IQR = Q3 – Q1, where Q1 is the 25th percentile and Q3 is the 75th percentile), the median, and whiskers that extend between Q1 -  $1.5 \times IQR$  to Q3 +  $1.5 \times IQR$ , beyond which points are typically flagged as statistical outliers. Certain points in the figure

extend beyond these whisker limits and may appear as outliers under the box-plot convention. However, upon incorporating facies information, it becomes evident that these points coincide with thin-bed facies transitions. Thus, rather than being statistical anomalies, they represent geologically significant variations. Removing such points would risk losing valuable information about facies heterogeneity. Since input variables often have different measurement scales, data transformation is applied to normalize all features to a uniform scale prior to model training. This preprocessing step facilitates faster convergence of ML algorithms and satisfies the requirements of certain modeling methods.

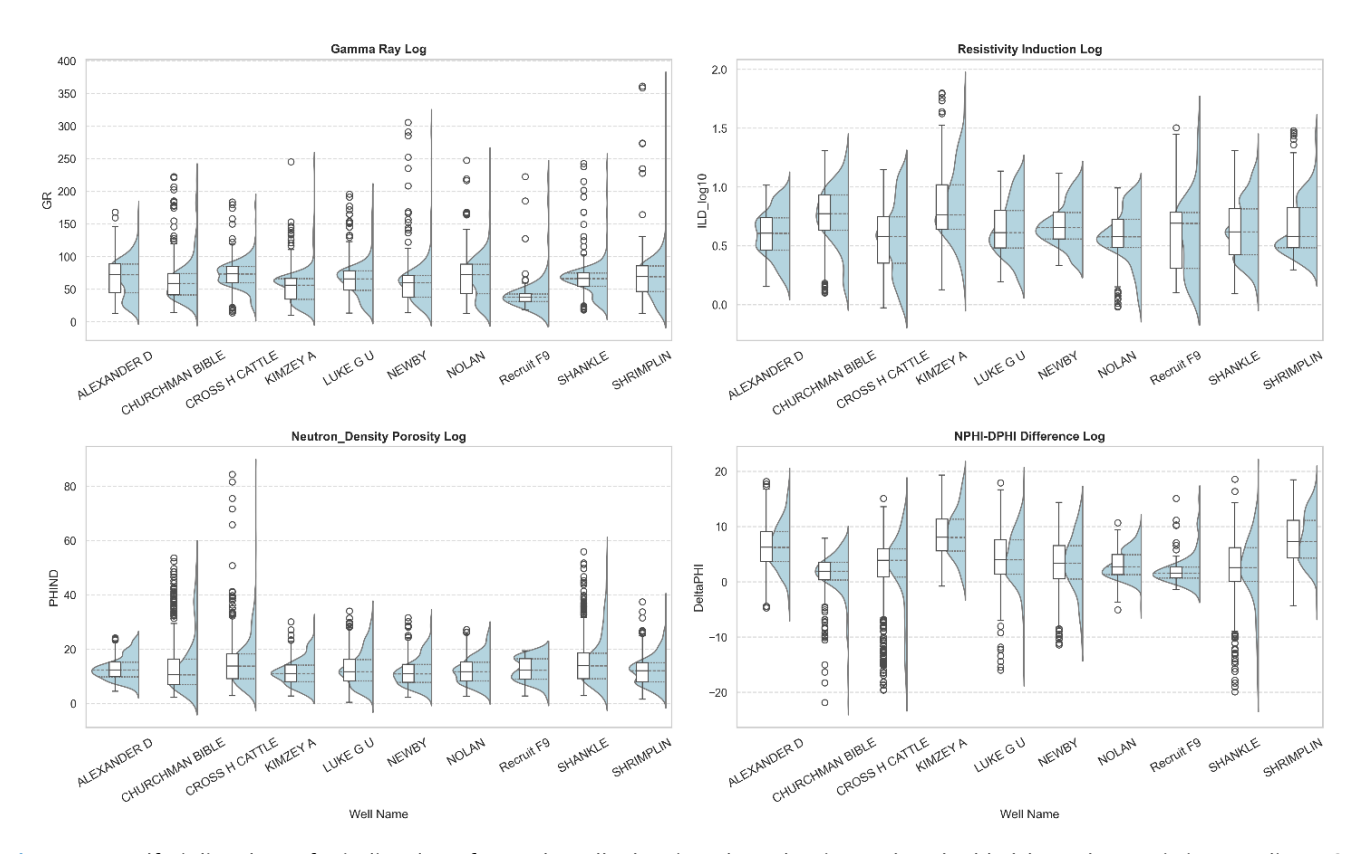


**Figure 5**: Half-violin plots of wireline logs for each well, showing data density and embedded box-plot statistics (median, IQR, whiskers). Points beyond whiskers may appear as outliers but often represent geologically significant variations reflecting subsurface heterogeneity.

Among five original wireline logs GR, ILD\_log10, PE, DeltaPHI, and PHIND, PE and GR are the best lithology predictors as observed from data visualization and histogram plots. Since the previous work of Dubois et al. (2007) and Hall (2016) did not achieve an exact facies accuracy of more than 50% on a blind well with the

wireline data, four more logs, namely, neutron porosity  $(\phi_N)$ , density porosity  $(\phi_D)$ , bulk density  $(\rho_b)$ , and volume of shale  $(V_{sh})$  have been computed from existing measurements to increase the number of input features. Matrix density values of each lithofacies are unique distinguishable physical properties as observed from

core measurements. Hence, we attempted to calculate continuous bulk density log, with an assumption of 100% brine-saturated rock ( $\rho_{fluid} = 1.0~g/cc$ ).

$$\varphi_N = \frac{1}{2}(2\varphi_{ND} + \Delta\varphi) \tag{1}$$

$$\varphi_D = \frac{1}{2}(2\varphi_{ND} - \Delta\varphi) \tag{2}$$

$$V_{sh} = \frac{GR - GR_{sand}}{GR_{shale} - GR_{sand}} \tag{3}$$

$$\rho_b = \left(1 - \frac{\varphi_{ND}}{100}\right)\rho_{ma} + \left(\frac{\varphi_{ND}}{100}\right)\rho_{fluid} \tag{4}$$

where  $\Delta \varphi$  refers to DeltaPHI,  $\varphi_{ND}$  is average neutrondensity porosity,  $GR_{sand}$  and  $GR_{shale}$  refer to sand and shale line respectively.  $\rho_{ma}$  and  $\rho_{fluid}$  represent matrix and fluid density respectively.

Incorporation of the above derived additional petrophysical logs could be beneficial to enhance the predictive accuracy of classification models compared to the existing wireline logs as reported in the literature (Lopes and Jorge, 2017). For the classification of lithofacies, we have used RF, MLP, and CNN-shift. A brief intuition behind each algorithm and its functioning is provided in Appendix-A.

For RF and MLP classifier, we chose to extract output that returns the probability estimates for each class label for a given input rather than standard majority voting system. In case of CNN-shift, "SoftMax" activation function outputs probability estimates over 0 to 1 scale for each class. Further, the prediction of probability for each feature class has been estimated, and quantification of facies with high confidence interval.

The confusion matrix and other statistical assessment metrics can be used to evaluate the classification accuracy of any predictive model (Powers, 2011). Several evaluation scores, including precision (P), recall (R), F1-score, and accuracy (A), were employed for model validation based on the confusion matrix.

$$A = \frac{TP + TN}{TP + FN + FP + TN} \tag{5}$$

$$P = \frac{TP}{TP + FP} \tag{6}$$

$$R = \frac{TP}{TP + FN} \tag{7}$$

$$F1 - score = 2 \times \frac{P \times R}{P + R}$$
 (8)

where TP, TN, FN, and FP refer to true positive, true negative, false negative, and false positive, respectively. For adjacent facies accuracy calculation, we have created an array to represent the facies adjacent to each other as defined in Table 1.

# **RESULTS AND DISCUSSION**

Eleven input features were utilized to predict target variables (lithofacies) from ten wells. Filling of PE logs in two wells increased the number of datasets from 3232 to 4,149. For facies classification out of 10 wells, 1 well was kept aside at a time to ensure robustness of blind testing and to generate accuracy score of the classifier between the predicted and actual facies labels. The remaining datasets were sliced into 80:10:10 proportions as training, validation, and testing sets, respectively. Supervised machine learning algorithms were applied to the training dataset with optimum hyperparameters to learn the mapping function between input features and the target facies classes.

We first evaluated model performance (cf. equation 5) using exact facies, where only predictions that match the true facies, are counted as correct, i.e., true positive (TP). However, since lithofacies are not strictly discrete and often display transitional characteristics, achieving perfect accuracy under this criterion is inherently difficult. To better reflect geological complexity, predictions were considered correct (true positives) if they matched either the true facies label or any of the geologically reasonable adjacent facies listed in Table 1. The metric scores considering only true facies predictions and those including adjacent facies predictions on blind data are summarized in Table 2 to identify the most reliable classifier. MLP and RF classifier algorithms show comparable metric scores, while the metric score of CNN-shift is lower than the two models. The results of the predicted facies output from the three models in comparison to the original facies distribution for the blind well testing are shown in Figure 6. Also, the predicted output results from the three models adjusted using the adjacent facies concept are shown in Figure 7. Upon comparing Figure 6 and Figure 7, one can notice that the metric score has increased significantly when using adjacent labels for prediction, as seen from the metric scores in Table 2. Hence, it is inferred that any of the mentioned classifiers is a suitable facies classifier model. For this case, MLP is selected for blind well facies prediction.

**Table 2**: Classification metric score for true facies (Original) and including geologically reasonable neighboring facies (Adjacent) for different blind well testing.

Model	odel Blind Well Accuracy		F1 Score		Recall		Precision		
		Original	Adjacent	Original	Adjacent	Original	Adjacent	Original	Adjacent
MLP	ALEXANDER D	0.82	0.96	0.82	0.97	0.82	0.97	0.81	0.97
	SHRIMPLIN	0.86	0.98	0.87	0.98	0.87	0.98	0.88	0.97
Average		0.84	0.97	0.845	0.975	0.845	0.975	0.845	0.97
RF	ALEXANDER D	0.80	0.95	0.79	0.96	0.8	0.96	0.79	0.96
	SHRIMPLIN	0.80	0.97	0.79	0.97	0.78	0.97	0.81	0.97
Average		0.80	0.96	0.79	0.965	0.79	0.965	0.8	0.965
CNN- Shift	ALEXANDER D	0.68	0.88	0.59	0.88	0.59	0.88	0.6	0.89
	SHRIMPLIN	0.65	0.94	0.66	0.95	0.65	0.95	0.64	0.95
Average		0.665	0.91	0.625	0.915	0.62	0.915	0.62	0.92

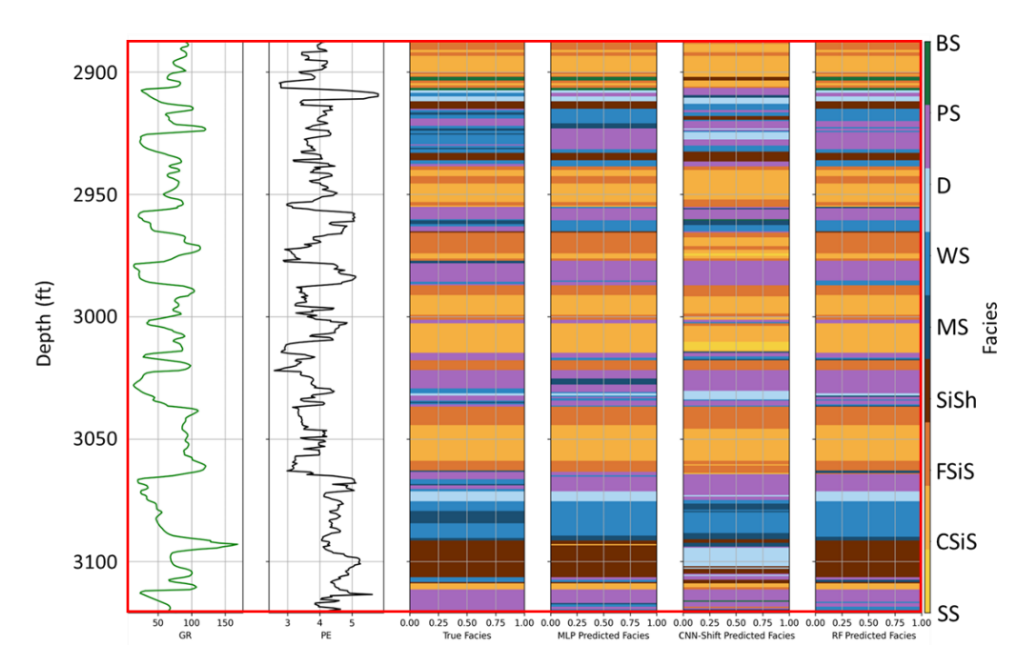


**Figure 6**: Gamma ray and photoelectric (PE) logs for the ALEXANDER D well in the first two tracks. Predicted facies from the MLP, CNN-shift, and RF models are shown alongside the true facies, with predictions made considering the true facies labels.

In a real geological setting, boundaries between facies are gradational rather than sharp; hence, it is important to know how confident the model is in its prediction at every depth. Hence, the probability of the predicted facies plot helps to identify these ambiguous zones, where the model hesitates between two or more facies. It helps to understand the cause behind the prediction of the facies by the model, which may be either because the facies truly dominate at a particular depth or there is a higher probability of that facies being present at that

depth among other facies with lower probabilities (Figure 8).

It becomes significant when determining the reliability of predictions in transition zones or thin layers. For example, in Figure 8, at slightly below 3000 ft, a thin layer transitioning from PS to WS, captured by MLP and RF algorithms with varying proportions. By comparing multiple models, we can visually assess which model has higher confidence, smoother transitions, or better alignment with the true facies (Figure 8).

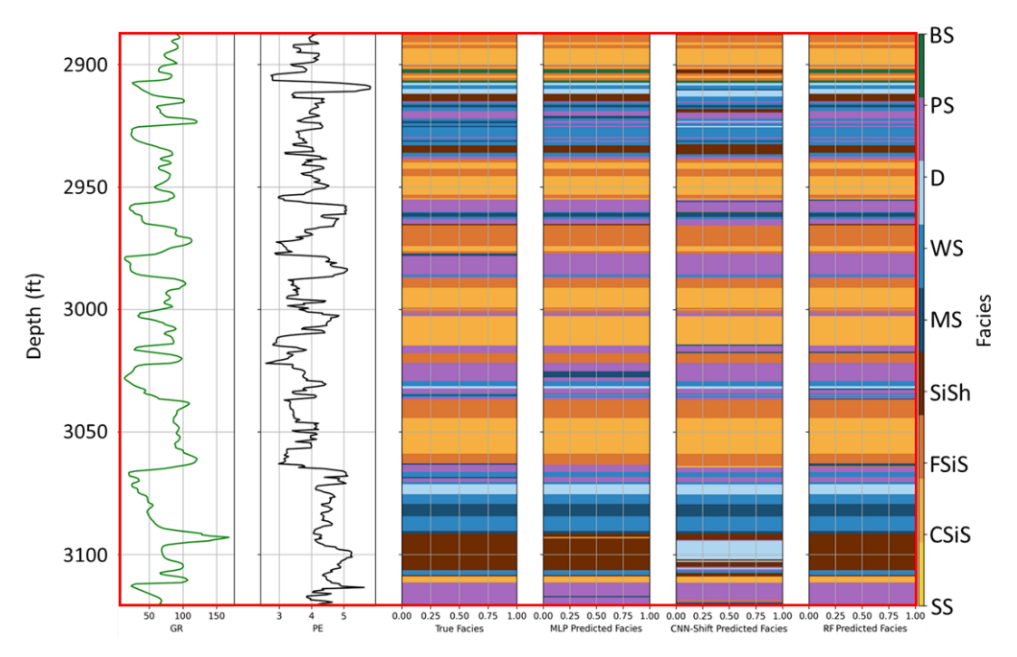


**Figure 7**: Gamma ray and PE logs for the ALEXANDER D well in the first two tracks. Predicted facies from the MLP, CNN-shift, and RF models are shown alongside the true facies, with predictions made considering the adjacent facies in labels.

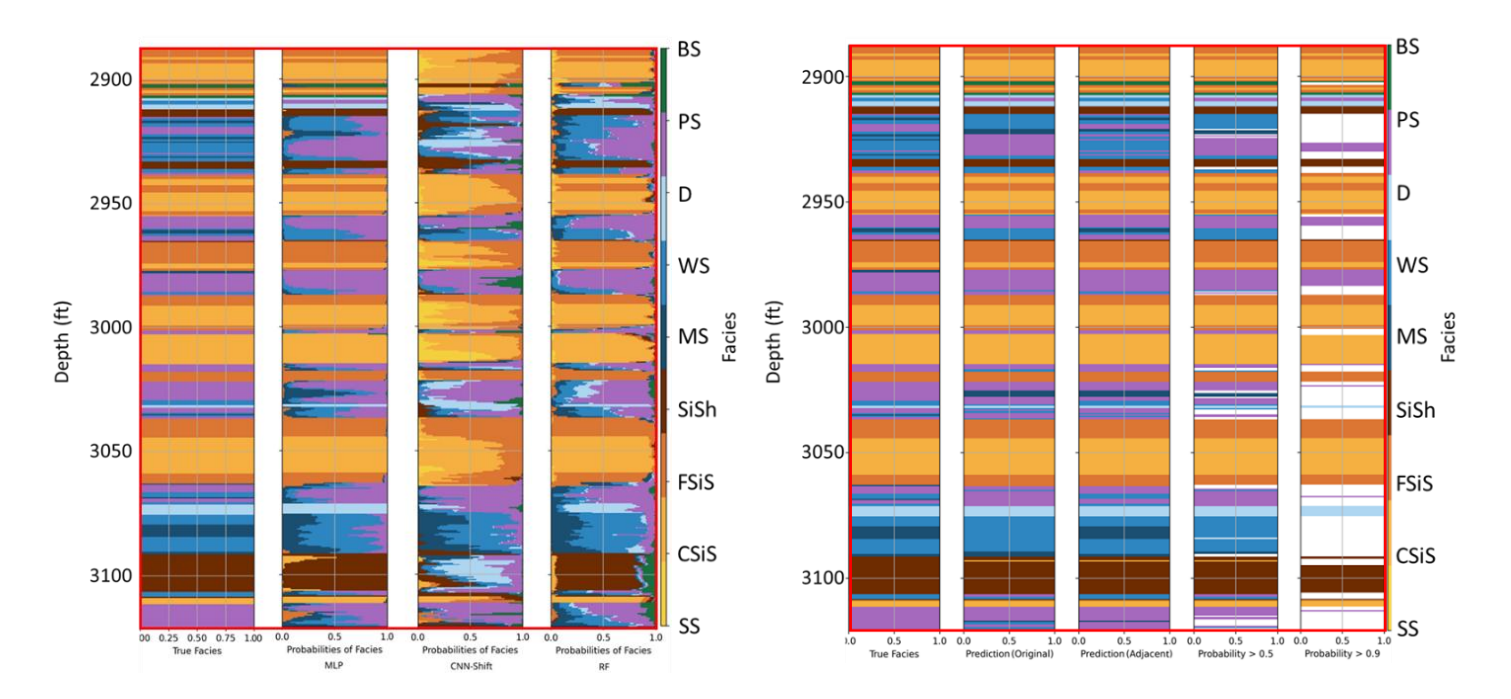


**Figure 8**: Predicted class probabilities for each facies are shown in tracks for the MLP, CNN-shift, and RF models, compared with the true facies for the ALEXANDER D well.

**Figure 9**: True facies alongside original and adjacent facies predictions using the MLP model for blind well – ALEXANDER D. Predictions are shown with probability thresholds at 50% and 90% confidence intervals. A reduction in classified facies is observed at the >90% confidence level.

Figure 9 shows the true facies, the original MLP predictions, and the predictions after including adjacent facies information. The last two columns display the predictions when only probabilities greater than 0.5 and 0.9 are considered. As the cutoff increases, more white spaces appear, meaning the model is less confident in those intervals. Mainly, the facies of Mudstone (MS), Wackstone (WS), and Packstone-Grainstone (PS) information are getting whitened as the probability cutoff increases, which means those facies predictions do not have much confidence. This highlights how using adjacent information improves predictions as well as

how probability thresholds help in identifying the most reliable results.

Figure 10 illustrates the performance and reliability of the MLP model using blind-well testing. The model was trained by leaving one well blind in each iteration to evaluate generalization. When ALEXANDER D was used as the blind well, the accuracy improved from 0.82 to 0.96 after incorporating adjacent facies information. Similarly, for SHRIMPLIN, the accuracy increased from 0.86 to 0.98 with the same adjustment, demonstrating the positive impact of contextual facies integration.

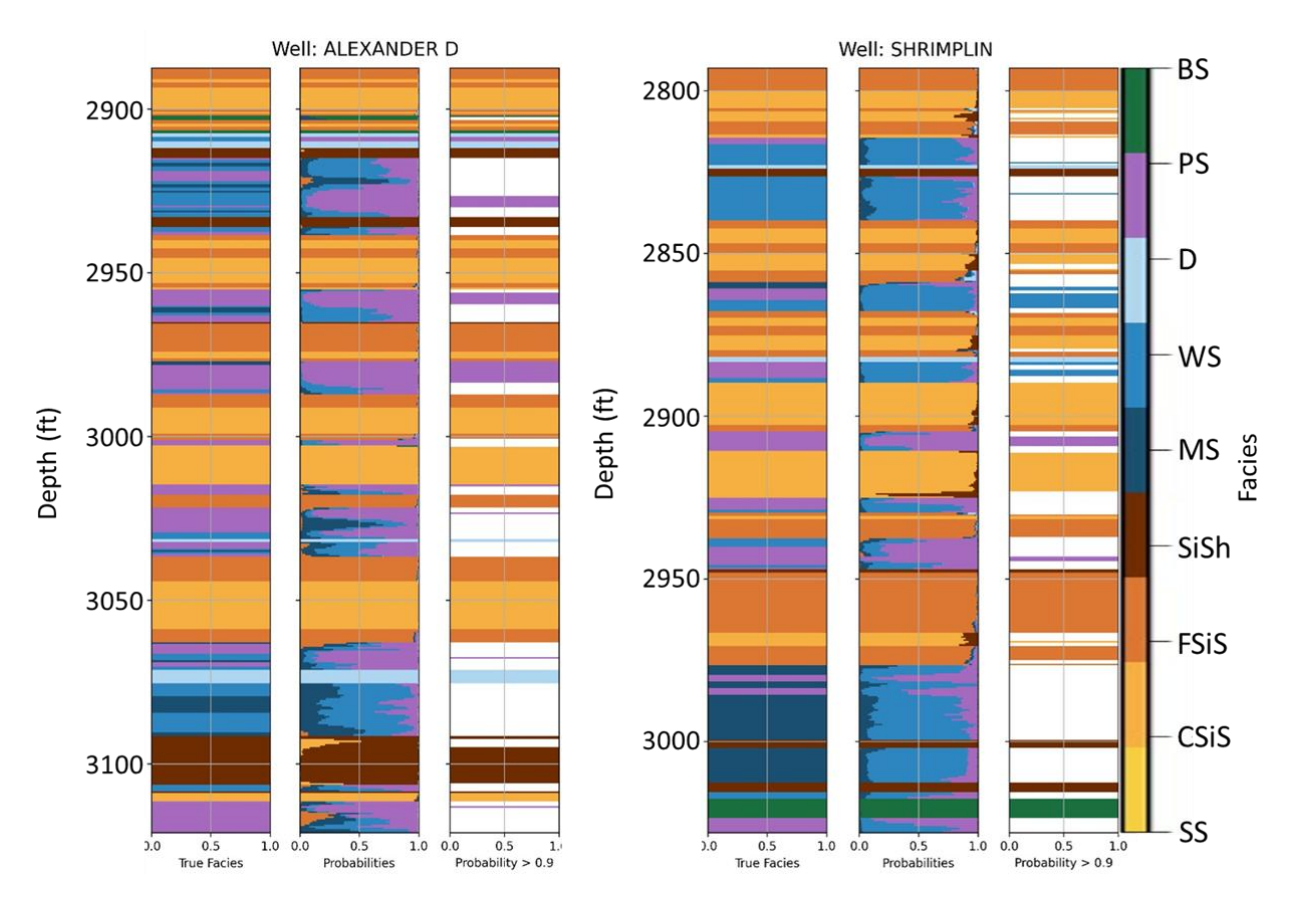


**Figure 10**: Blind well prediction comparison between the ALEXANDER D and SHRIMPLIN wells. In the plots, intervals where predicted probabilities for any facies classes did not exceed a 90% confidence level are left blank, while intervals with probabilities higher than 90% are displayed. This representation highlights that the MLP model demonstrates good generalization performance.

Several important observations can be made from the results:

- Accurate prediction of Marine Siltstone and Shale (SiSh): The model consistently identifies the SiSh
- facies with high accuracy, even for thin beds, closely matching the true facies distribution.
- Reliable detection of Phylloid-Algal Bafflestone (BS): Despite the limited number of BS samples(Figure 1), the model successfully predicts

very thin BS layers (e.g., ~2900–2950 ft in ALEXANDER D and ~2800–2850 ft and ~3000–3050 ft in SHRIMPLIN) with probabilities exceeding 90%. This is particularly significant since BS represents potential gas-bearing facies.

- 3. Confusion between Non-Marine Coarse Siltstone (CSiS) and SiSh: Some misclassification occurs where small probabilities of SiSh are assigned to CSiS intervals, even though the two are not adjacent facies. However, given that both are siltstone-dominated lithologies, this overlap is reasonable. Importantly, the model still distinguishes CSiS from SiSh with sufficient probability resolution, indicating robustness in handling transitional or thin-bed facies.
- 4. Uncertainty in MS–WS–PS transitions: Most of the white intervals in the >90% probability plots correspond to zones dominated by Mudstone (MS), Wackestone (WS), and Packstone–Grainstone (PS). Around 3000 ft in both wells, these facies exhibit nearly equal probability distributions without any class exceeding the 90% threshold. Since these facies occur in adjacent transitions (MS → WS → PS) (Table 1), the model exhibits ambiguity, reflecting genuine geological similarity rather than random misclassification.

By the addition of more input features including PE and bulk density logs as well as increasing number of training samples, substantial improvement of model's prediction performance have been achieved compared to results from MLP and SVM algorithm reported in previously published works (Dubois et al., 2007; Hall, 2016). Overall, the results confirm that the MLP model has captured both thick and thin facies distributions with high reliability, while probability thresholding provides insight into facies-specific uncertainties and confidence levels.

# **CONCLUSIONS**

In this study, we demonstrated the advantages of capturing facies class transition by adopting probabilistic facies classification through the application of multiple machine learning algorithms. Based on classification metrics performance on blind test (accuracy of 0.82 and 0.86, and F1-score of 0.82 and 0.87).

for ALEXANDER D and SHRIMPLIN, respectively), Multilayer Perceptron (MLP)- an ANN algorithm outperformed the remaining Random Forest (RF) and Convolutional neural network (CNN) classifier. Probabilistic driven classification output in the range of 0 to 1 scale not only resolved geologically meaningful transition of facies but also mapped one of the prominent gas-bearing facies, Phylloid-Algal Bafflestone (BS) in the Hugoton gas field which could be beneficial for subsurface modelling.

#### **ACKNOWLEDGEMENTS**

The authors would like to thank the Kansas Geological Society (KGS) for the availability of datasets and existing reports used in this work. Members of the subsurface resource characterization group (sRCg), Department of Applied Geophysics, are acknowledged for their support and motivation to complete this work. Authors are also thankful to the IIT(ISM) Dhanbad for providing the necessary research environment and computational facility to conduct this study.

# **APPENDIX**

#### Random Forest (RF)

Random Forest is an ensemble learning method that constructs a number of decision trees and combines their outputs to improve predictive performance (Breiman, 2001). Each tree is trained on a bootstrap sample (random subset) of the training data, and at every split, only a random subset of features is considered. This dual randomness, data sampling, and feature selection reduces variance and helps prevent overfitting compared to a single decision tree.

For regression tasks, the predictions from individual trees are averaged to obtain the final continuous output. For classification tasks, each tree casts a "vote" for the predicted class, and the final class is chosen by majority voting and probability across all trees. This aggregation mechanism allows Random Forest to produce stable, generalizable, and robust predictions in both categorical and continuous settings, making it effective even in the presence of noise or highly variable data.

# *Multilayer Perceptron (MLP)*

The Multilayer Perceptron is a feedforward artificial neural network (ANN) that models complex nonlinear

relationships between input features and output classes (Rumelhart et al., 1986). It consists of an input layer, one or more hidden layers, and an output layer, where each neuron applies a weighted linear transformation followed by a nonlinear activation function. During training, the network learns hierarchical feature representations through backpropagation, in which errors are propagated backward, and weights are updated using gradient descent to minimize a predefined loss function. By stacking multiple layers, MLPs can capture intricate patterns in geological data, enabling effective lithofacies classification.

# Convolutional Neural Network with Shift padding (CNN-shift)

The Convolutional Neural Network with shift modification extends conventional CNNs to capture spatially correlated patterns in sequential data such as well logs and seismic traces (Lecun et al., 1998; Wei et al., 2019). CNNs operate by applying convolutional filters across the input to detect local features, followed by pooling operations that reduce dimensionality while preserving essential information. The "shift" mechanism incorporates shifted windows or neighbouring slices of data, enhancing the model's ability to detect lithofacies transitions and stratigraphic continuity. Extracted features are then passed through fully connected layers to map them into lithofacies probability classes, making CNN-shift particularly effective for identifying facies boundaries in depth-dependent datasets.

Since well log responses are one-dimensional arrays (e.g., Gamma Ray or ILD\_log10), applying 2D convolution directly is not possible. To enable the use of Conv2D, the 1D log sequences must be transformed into a two-dimensional representation. This is achieved through the *shift padding method*, where the original log values are arranged into overlapping shifted sequences. Each subsequent row is a circularly shifted version of the initial 1D array, so that local depth patterns and neighbouring variations are spatially embedded in a 2D grid. This structured transformation captures both vertical continuity and lateral shifts within the data, allowing CNN filters to extract important spatial features from well logs that would otherwise be lost in a pure 1D formulation.

SoftMax activation function is used in the output layer of the CNN network, which helps us with multi-class classification. This activation function produces a probability distribution across all classes (sums to 1). The equation of the activation function is given as

$$\sigma(z_i) = \frac{e^{z_i}}{\sum_{j=1}^k e^{z_j}}, \text{ for } i = 1, 2, ..., k$$
 (9)

where,  $z_i$  = input score (logit) for class i, k = total number of classes,  $\sigma(z_i)$  = probability of class i.

#### **REFERENCES**

Breiman, L., 2001, Random Forests: Machine Learning, **45**, 5–32, <a href="https://doi.org/10.1023/A:1010933404324">https://doi.org/10.1023/A:1010933404324</a>.

Carr, T., and R. S. Sawin, 1997, Hugoton Natural Gas Area of Kansas, Public Information Circular.

Hemsell, C. C., 1939, Geology of Hugoton Gas Field of Southwestern Kansas, AAPG Bulletin, **23** (7),1054-1067. https://doi.org/10.1306/3D9330DA-16B1-11D7-8645000102C1865D

Dubois, M. K., G. C. Bohling, and S. Chakrabarti, 2007, Comparison of four approaches to a rock facies classification problem: Computers & Geosciences, **33(5)**, 599–617, https://doi.org/10.1016/j.cageo.2006.08.011.

Dubois, M. K., A. P. Byrnes, G. C. Bohling, and J. H. Doveton, 2006, Multiscale geologic and petrophysical modeling of the giant Hugoton Gas Field (Permian), Kansas and Oklahoma, U.S.A., in Giant Hydrocarbon Reservoirs of the World: From Rocks to Reservoir Characterization and Modeling, American Association of Petroleum Geologists, https://doi.org/10.1306/1215881M883274

Dunham, R. J., 1962, Classification of carbonate rocks acccording to depositional texture, in classification of carbonate rocks—A Symposium, American Association of Petroleum Geologists.

Hall, B., 2016, Facies classification using machine learning: The Leading Edge, **35**(10), 906–909.

https://doi.org/10.1190/tle35100906.1.

Halotel, J., V. Demyanov, and A. Gardiner, 2020, Value of geologically derived features in machine learning facies classification: Mathematical Geosciences, **52**, 5–29, <a href="https://doi.org/10.1007/s11004-019-09838-0">https://doi.org/10.1007/s11004-019-09838-0</a>

Lecun, Y., L. Bottou, Y. Bengio, and P. Haffner, 1998, Gradient-based learning applied to document recognition: Proceedings of the IEEE, **86**(11), 2278–2324.

https://doi.org/10.1109/5.726791

Lopes, R. L., and A. M. Jorge, 2017, Mind the gap: A well log data analysis, *in* Proceedings of the Workshop on Data Mining for Oil and Gas (DM4OG), arXiv:1705.03451

Mazzullo, S.J., 1998, Stratigraphic architecture of Lower Permian, cyclic carbonate reservoirs (Chase Group) in the Mid-Continent USA, based on outcrop studies, AAPG Bulletin, **82**(3), 464-483. <a href="https://doi.org/10.1306/1D9BC43F-172D-11D7-8645000102C1865D">https://doi.org/10.1306/1D9BC43F-172D-11D7-8645000102C1865D</a>

Olson, T. M., J. A. Babcock, K. V. K. Prasad, S. D. Boughton, P. D. Wagner, Franklin, and K. A. Thompson, 1997, Reservoir characterization of the giant Hugoton Gas Field, Kansas: AAPG Bulletin, **81**(11), 1785-1803.

https://doi.org/10.1306/3B05C62C-172A-11D7-8645000102C1865D

Powers, D. M. W., 2011, Evaluation: from precision, recall and F-measure to ROC, informedness, markedness and correlation, Journal of Machine Learning Technologies, **2**. 37-63, http://www.bioinfo.in/contents.php?id=51

Rumelhart, D. E., G. E. Hinton, and R. J. Williams, 1986, Learning representations by back-propagating errors, Nature, **323**, 533–536, <a href="https://doi.org/10.1038/323533a0">https://doi.org/10.1038/323533a0</a>

Wei, Z., H. Hu, H. Zhou, and A. Lau, 2019, Characterizing rock facies using machine learning algorithm based on a convolutional neural network and data padding strategy, Pure and Applied Geophysics, **176**(8), 3593–3605, <a href="https://doi.org/10.1007/s00024-019-02152-0">https://doi.org/10.1007/s00024-019-02152-0</a>.

#### **BIOGRAPHIES**



**Tanmay Singh** is a Ph.D. scholar in the Department of Applied Geophysics at the Indian Institute of Technology (ISM), Dhanbad. He earned his Bachelor of Science in physics from Banaras Hindu University, Varanasi, followed by a master's in applied geophysics from IIT (ISM), Dhanbad. His doctoral research focuses on the exploration of natural hydrogen, combining field-based insights with advanced data-driven techniques. His academic journey has been enriched by extensive field training in geophysics, alongside developing strong technical skills. He is proficient in Python programming, which he applies to geophysical data analysis, critical mineral mapping with machine learning, and reservoir simulation. He also has experience with ArcGIS, Geovation, and Geosoft, and is highly skilled in the Microsoft Office suite for data management and reporting. His professional interests lie in petrophysics, subsurface data analysis, and integrating computational methods with geoscience to develop practical solutions for geophysical exploration.



**Pradyut Laha** is an aspiring geoscientist with a strong interest in petrophysics, seismic analysis, machine learning, and Al. He is currently pursuing an M.Sc. Tech. in applied geophysics at the Indian Institute of Technology (ISM), Dhanbad, after completing a B.Sc. in physics from Bankura University, West Bengal. His thesis focuses on seismic-driven 3D pore pressure cube prediction by integrating seismic attributes with well data. His academic journey has been enriched through hands-on field training in geophysics and industry-focused internships. At Halliburton, he worked on seismic data interpretation and workflow preparation using Decision Space Geosciences (DSG). Pradyut's technical expertise spans strong proficiency in Python, Microsoft Office, and PowerPoint, intermediate experience with Decision Space Geosciences, and a foundational understanding of Petrel. He has been recognized for his academic excellence with the ONGC and Institute Merit Scholarships.



**Nabin Mandal** is an aspiring geophysicist with a keen interest in petrophysics, rock physics, geomechanics and core analysis. He is currently pursuing M.Sc. Tech. in applied geophysics at IIT (ISM) Dhanbad, following B.Sc. (Hons) in physics from Durgapur Government College, West Bengal. He served in WIHG, Dehradun as a summer intern where he worked on estimating TOC through synergistic implementation of conventional empirical equations and ML algorithms as a case study in KG Basin. He is skilled in data-driven approaches in formation evaluation and electro-facies classification. His technical expertise includes Python, Scikit-Learn and foundational understanding of Petrel and ArcGIS. His master thesis work focuses on developing a joint inversion framework that integrates multiple geophysical datasets incorporating empirical rock physics equations for serpentinization and natural

hydrogen exploration. He had served as a content writer in IGU Student Chapter and participated in ETES Conference at IIT (ISM) Dhanbad as an anchor. He has been recognized with the prestigious ONGC Scholarship.



**Prof. Partha Pratim Mandal** is an Assistant Professor in the Department of Applied Geophysics, IIT(ISM) Dhanbad, where he teaches borehole logging tools, formation evaluation, and energy geomechanics units. He holds a Ph.D. degree from Curtin University, Australia, and earned M.Sc. Tech in applied geophysics from ISM, Dhanbad. Prior to that he received B.Sc. in Physics (Hons) from Presidency College, University of Calcutta, West Bengal, India. In addition, he serves as a visiting scientist fellow at CSIRO Energy, Australia, and technical advisor at Qeye.

The primary focus of his research is petrophysics, rock-physics, and geomechanics for hydrocarbon exploration and development, energy transition (CO<sub>2</sub> sequestration, natural hydrogen), critical minerals mapping with AI techniques. He leads the Subsurface Resource Characterization Group, to support natural resource characterization and innovative subsurface modelling technology development in

energy transition projects. He is also the faculty advisor for the SPWLA student chapter, a committee member at the Centre for Hydrogen and CCUS Technologies at IIT(ISM) Dhanbad and active member of SEG and SPWLA.



Fault-bend fold in Kioto Limestone at Kibber Village, Spiti-Zanskar Basin. (Photo courtesy: Syed Shadab Ahmed and Deepak Rawat, ONGC)